The EMBO Journal (2012) 31, 503–514 | © 2012 European Molecular Biology Organization | Some Rights Reserved 0261-4189/12
www.embojournal.org

THE EMBO JOURNAL

EMBO open

Regulation of translocation polarity by helicase domain 1 in SF2B helicases

Robert A Pugh[1,2], Colin G Wu[1] and Maria Spies[1,2,3,*]

[1]Department of Biochemistry, University of Illinois at Urbana-Champaign, Urbana, IL, USA, [2]Howard Hughes Medical Institute, University of Illinois at Urbana-Champaign, Urbana, IL, USA and [3]Center for Biophysics and Computational Biology, University of Illinois at Urbana-Champaign, Urbana, IL, USA

Structurally similar superfamily I (SF1) and II (SF2) helicases translocate on single-stranded DNA (ssDNA) with defined polarity either in the 5′–3′ or in the 3′–5′ direction. Both 5′–3′ and 3′–5′ translocating helicases contain the same motor core comprising two RecA-like folds. SF1 helicases of opposite polarity bind ssDNA with the same orientation, and translocate in opposite directions by employing a reverse sequence of the conformational changes within the motor domains. Here, using proteolytic DNA and mutational analysis, we have determined that SF2B helicases bind ssDNA with the same orientation as their 3′–5′ counterparts. Further, 5′–3′ translocation polarity requires conserved residues in HD1 and the FeS cluster containing domain. Finally, we propose the FeS cluster-containing domain also provides a wedge-like feature that is the point of duplex separation during unwinding.

The EMBO Journal (2012) **31,** 503–514. doi:10.1038/emboj.2011.412; Published online 11 November 2011
Subject Categories: genome stability and dynamics
Keywords: DNA helicase; protein–DNA interaction; translocation polarity; Nucleotide Excision Repair; XPD

Introduction

Helicases are motor proteins that use the chemical energy of NTP binding and hydrolysis to move directionally on nucleic acid lattices. Translocation polarity is a predefined, inherent feature for each particular enzyme and reflects helicase movement either in the 3′–5′ or in the 5′–3′ direction (Singleton *et al*, 2007). Cellular activities of all *bona fide* !DNA helicases stem from their directional translocation. Defining the mechanism by which superfamily II (SF2) helicases adopt translocation polarity has proven elusive due to the absence of structural information on the complex of a 5′–3′ helicase (SF2B) bound to DNA. Superfamily I (SF1) and SF2 helicases translocate in either 3′–5′ (denoted as SF1A and SF2A) or 5′–3′ (SF1B and SF2B) direction using structurally identical motor cores defined by similar sets of conserved helicase signature motifs (Singleton *et al*, 2007; Fairman-Williams *et al*, 2010).

*Corresponding author. Department of Biochemistry, University of Illinois at Urbana-Champaign, RAL493, 600 S. Mathews Avenue, Urbana, IL 61801-3602, USA. Tel.: +1 217 244 9493; Fax: +1 217 244 5858; E-mail; mspies@life.illinois.edu

Received: 1 July 2011; accepted: 21 October 2011; published online: 11 November 2011

Recent structural studies suggested the mechanism underlying polarity of translocation in SF1 helicases (Singleton *et al*, 2004; Saikrishnan *et al*, 2008, 2009). The motor core of SF1A enzymes consists of two RecA-like folds, 1A and 2A (Figure 1A), where domain 1A contacts the 3′-end of the occluded ssDNA and domain 2A faces the 5′-end (Figure 1A, top). It has been accepted that all SF1A helicases bind DNA with the same orientation and translocate using the same sequence of conformational changes within the motor regulated by binding and hydrolysis of ATP (Soultanas and Wigley, 2000). The translocation strand bound in the cleft, which spans both domains 1A and 2A, makes extensive contacts with residues interacting with the bases of the bound nucleotide.

The binary complex of RecD from *D. radiodurans* (SF1B helicase) bound to an 8mer ssDNA revealed that the helicase interacts with the first four nucleotides of the 5′-end using domain 2A while the four nucleotides of the 3′-end interact with the 1A domain as depicted in Figure 1A (bottom) (Saikrishnan *et al*, 2009). As a result, both SF1A and SF1B helicases bind to the translocating strand with the same orientation. Polarity is the result of a predefined sequence of the conformational changes induced by ATP binding and hydrolysis, which is reversed in the SF1B enzymes compared with SF1A. One significant difference between SF1A and SF1B helicases bound to ssDNA is that the key residues involved in translocation interact with the backbone of DNA for SF1B as opposed to base interactions observed for SF1A. For SF1 enzymes, a distinction can be made between 3′–5′ and 5′–3′ enzymes in signature helicase motif Ia, which contains a conserved phenylalanine for SF1A helicases. A proline found in the corresponding position in SF1B enzymes opens a binding pocket to be occupied by a base from the translocating strand (Saikrishnan *et al*, 2008). A proline in this motif is also found in SF2A helicases, however, a conserved arginine and threonine are found in motif Ia in SF2B helicases (Pugh *et al*, 2008a). Additionally, the two highly conserved threonine residues typically found in motifs Ic and V of SF1 and SF2 helicases that separate nucleic acid duplexes by translocation are absent in SF2B helicases (Fairman-Williams *et al*, 2010).

Similarly to SF1 enzymes, the motor core of SF2 helicases comprise two RecA-like folds, helicase domain 1 (HD1) and helicase domain 2 (HD2) which are equivalent to helicase domains 1A and 2A, respectively (Figure 1B; Singleton *et al*, 2007; Fairman-Williams *et al*, 2010). Several structures are currently available for SF2A helicases bound to nucleic acids (Kim *et al*, 1998; Buttner *et al*, 2007; Luo *et al*, 2008) and for dsDNA translocating motors (Thoma *et al*, 2005). These structures show HD2 bound to the 5′-end of the oligonucleotide and HD1 to the 3′-end (Figure 1B, top). Only apo structures are currently available for SF2B enzymes (Fan *et al*, 2008; Liu *et al*, 2008; Wolski *et al*, 2008).

Identifying the orientation of XPD bound to DNA is a prerequisite for establishing how directional translocation is

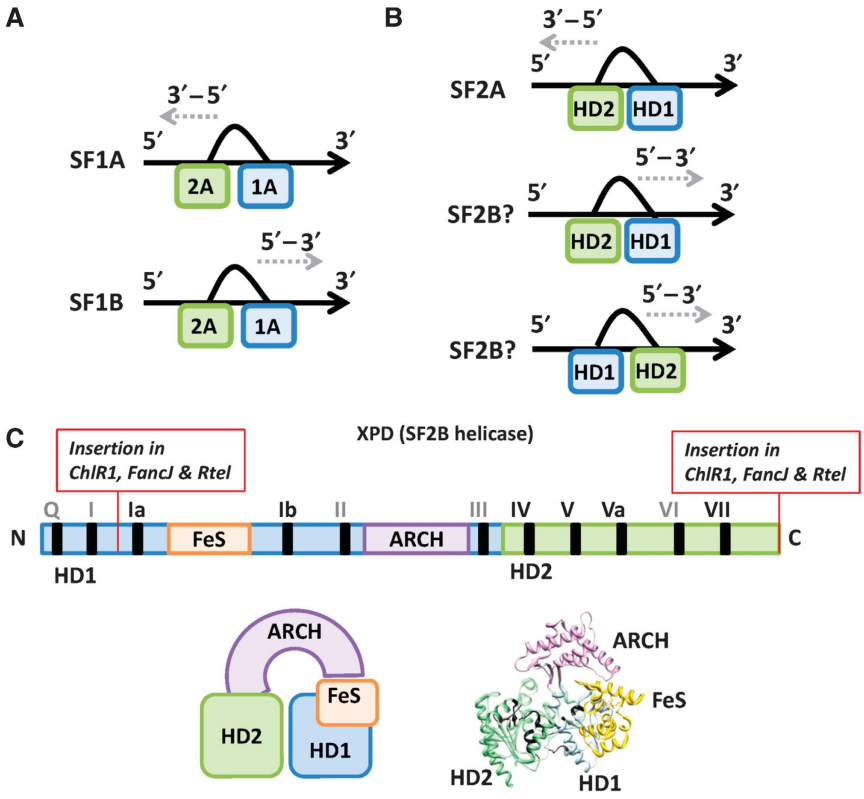

Figure 1 Orientation of SF1 and SF2 helicases bound to ssDNA: (**A**) Schematic representation of the mechanism underlying polarity of SF1 helicases. Upon binding to ssDNA, domain 2A of SF1 helicases interacts with the 5′-end of occluded ssDNA and 1A interacts with the 3′-end. These enzymes translocate in either the 3′–5′ direction with HD2 as the leading fold or 5′–3′ with 1A being the leading fold. (**B**) SF2A helicases translocate 3′–5′ with the same orientation as SF1 helicases. In order to translocate in the 5′–3′ direction, the helicase will either bind DNA with the same orientation and reverse the conformational change between the motor domains (middle), or it may bind to DNA with the opposite orientation but maintain the relative orientation of the motor subunits with HD2 being the leading fold (bottom). (**C**) Primary structure (top) and domain organization (bottom) of XPD helicase from *T. acidophilum*. Modular domains are colour coded as HD1 (blue), HD2 (green), Arch (purple) and FeS (orange). Modular insertions characteristic to eukaryotic ChlR1, FancJ and Rtel helicases are indicated by red rectangles. Helicase signature motifs are shown as black bars and roman numerals on the primary structure. Motifs directly involved in DNA binding are highlighted in black on the ribbon representation of *Tac*XPD (pdb: 2VSF).

determined in SF2 helicases. Two mutually exclusive models can be proposed to explain reversal of translocation polarity in SF2B helicases (Figure 1B). A helicase may bind ssDNA with the same orientation as SF1 and SF2A helicases, then translocate in the opposite direction by reversing the ATP-driven conformational changes within the motor (Figure 1B, middle). Alternatively, a 5′–3′ helicase would bind to DNA with the opposite orientation compared with SF1A and SF2A helicases and translocate in the opposite direction by maintaining the same molecular motor movement as SF2A enzymes (Figure 1B, bottom). The first model is consistent with the mechanism by which translocation polarity is reversed in SF1 helicases. The second model is consistent with the difference between motif 1a in SF2B helicases compared with that of the SF1A enzymes. In contrast to their SF1 counterparts, both SF2A and SF2B helicases are believed to interact with the phosphodiester backbone of their respective lattices. This has been demonstrated for SF2A helicases through structural studies (Kim *et al*, 1998; Buttner *et al*, 2007; Luo *et al*, 2008) and inferred for SF2B enzymes from their ability to bypass damaged bases (Rudolf *et al*, 2010) and ssDNA binding proteins that specifically interact with the bases (Honda *et al*, 2009).

Only a limited number of SF2B helicases have been identified, all of which belong to the Rad3 family comprising XPD (Rad3), Rtel, FancJ, DinG and ChlR1 (White, 2009; Wu *et al*, 2009). All helicases in this family are involved in DNA repair and in maintenance of the genetic integrity. Here, we used XPD from *Thermoplasma acidophilum* to determine how polarity is defined in SF2 helicases. In humans, XPD is one of the two helicases of the TFIIH complex, which is involved in transcription initiation and nucleotide excision repair (NER; Egly and Coin, 2011). The helicase activity of XPD is dispensable for its role in transcription initiation (Dubaele *et al*, 2003). It, however, is required for NER (Coin *et al*, 2007). XPD is composed of four domains (Fan *et al*, 2008; Liu *et al*, 2008; Wolski *et al*, 2008). The modular motor core consists of HD1 and HD2. Two additional domains, FeS and Arch, are found within HD1 (schematically depicted in Figure 1C). The FeS domain is stabilized by the presence of a 4Fe-4S cluster and the Arch domain represents a unique structural fold. The Arch domain sits above the two helicase motor domains, and forms a donut-like structure with a central pore between the FeS domain and HD1 where ssDNA is proposed to pass (Fan *et al*, 2008; Liu *et al*, 2008; Wolski *et al*, 2008).

Previously, we suggested that XPD binds to a forked DNA or to its natural bubble-like substrate so that the FeS domain is involved in strand separation (Pugh *et al*, 2008a). Implicit in this model was XPD binding the translocating strand with

the same orientation as SF1 and SF2A helicases. Two mutually exclusive orientations of ssDNA, however, were proposed based on the crystal structures (Fan *et al*, 2008; Liu *et al*, 2008; Wolski *et al*, 2008). Here, we set out to provide direct evidence for bound ssDNA orientation and to identify the path of the translocation strand through the helicase.

To test these two proposed translocation models, we probed XPD–ssDNA complex using Fe(III) (s)-1-(*p*-bromoacetamidobenzyl) ethylenediamine tetraacetic acid (FeBABE), a hydroxyl radical generating moiety that was site specifically incorporated into 12mer ssDNA. Using the reverse footprinting technique (reviewed in Meares *et al*, 2003), we have determined that polarity in SF2 helicases is accomplished similarly to SF1 helicases.

After confirming the binding orientation, we hypothesized that contacts from HD1 and the FeS domain with the translocating strand of the DNA substrate would play an important role in controlling XPD translocation. Mutational analysis was conducted to identify key residues in domains HD1 and FeS of XPD and their influence on duplex unwinding activity was examined. We have identified two aromatic residues near the FeS cluster that may serve as a wedge for initiating duplex separation. Finally, five positively charged residues and a histidine contributed by FeS and HD1 domains positioned to interact with the 3′-end of the translocating strand are important for either promoting or inhibiting substrate unwinding by XPD helicase, implicating these residues in the interaction with the translocating strand on its path between the motor core and duplex separation site. The model is set forward whereby these interactions restrict XPD processivity distinguishing it from more processive helicases in the family (such as FancJ and Rtel).

Results

FeBABE mediated proteolytic cleavage of XPD helicase

In order to determine the orientation of DNA when bound by XPD, the artificial protease, FeBABE, was chemically incorporated into a DNA oligonucleotide containing phosphorothioate linkages positioned along the DNA backbone during oligonucleotide synthesis creating a proteolytic DNA (Schmidt and Meares, 2002). In the presence of ascorbic acid and H_2O_2, a hydroxyl radical is generated. The hydroxyl radical diffuses and cleaves the peptide backbone generating protein cleavage fragments. Cleavage sites can be assigned with high precision by comparing mobility of the FeBABE-produced fragments with chemical digests generated from the same protein (Owens *et al*, 1998).

*Tac*XPD helicase containing an N-terminal 6 × His tag and a C-terminal FLAG tag was purified to homogeneity (Supplementary Figure S1A). A series of 12mer ssDNA oligonucleotides were labelled with FeBABE at a single position on the backbone in between bases as numbered from the 5′-end. Protein fragments were resolved by SDS–PAGE and visualized by western blots to map the distance between the two termini of the XPD polypeptide and the cleavage sites (Figure 2A and B; Supplementary Figure S2A and B). Each fragment was assigned a residue based upon its molecular weight as determined by the distance migrated on the gel as described in Materials and methods (Supplementary Table S1).

FeBABE mediated cleavage indicates the orientation of XPD bound to DNA

Using a series of 12mer ssDNA substrates each containing a single FeBABE modification (schematically depicted over corresponding lanes in Figure 2 and Supplementary Figure S2), we expected to observe a change in the unique fragments generated by hydroxyl radicals. The length of the FeBABE-conjugated DNA substrates was shorter than 20 nucleotides occluded by primary and secondary DNA binding sites of XPD helicase (Honda *et al*, 2009) to ensure that we achieve the cleanest distribution of cleavage sites. When mapped on the structure of XPD, the change in the cleavage pattern should reveal the orientation of XPD when bound the substrate, and the path of DNA through the helicase. Cuts generated using substrates with FeBABE near the 5′-end of ssDNA appear in HD2 and in the Arch domain above HD2 (Figure 3A), placing the 5′-end of DNA in contact with HD2. Specifically, substrate (1) produced fragments on α-helix 22 in HD2 and β-strand 7 in the Arch domain; α-helix 22 in HD2 forms the floor of the channel where the translocation strand is expected to bind as the helicase translocates away from the 5′-end; β-strand 7 is located above α-helix 23 forming the top of the channel for ssDNA binding; substrates (2) and (3) produced cuts in the N-terminal region of α-helix 24, while substrates (1) and (4) cut on the C-terminal end of α-helix 24 on helicase motif VI (Figure 3A); α-helix 24 runs parallel to helicase motifs V, which is known to interact with DNA (Pyle, 2008) and motif Va which has been implicated in DNA binding (Liu *et al*, 2008). The position of these cuts is consistent with the 5′-end of the translocating strand interacting with highly conserved residues found within the DNA binding motifs as they map directly adjacent to these motifs. No cuts were observed in HD1 or FeS domain.

Hydroxyl radical cleavage resulting from centrally positioned FeBABE yielded cuts in all four domains (Figure 3B). A majority of the cuts were observed in HD2. Cleavage products were mapped on α-helix 19 for substrates (5–7) and α-helix 20 for substrates (5) and (6). These two helices sandwich helicase motif IV, a DNA binding motif (Pyle, 2008). Substrates (5–7) also cleave the protein on the loop between α-helices 20 and 21 adjacent to helicase motif IV. α-Helix 21 runs along the ATP binding cleft between HD2 and HD1. N-terminally, this helix is cleaved by substrates (5) and (7) while C-terminal cuts are generated by (5) and (6). The loop between α-helix 21 and β-strand 14 is also cleaved by substrates (5) and (6). A loop running between β-strand 15 and α-helix 22 that contains helicase motif Va implicated in DNA binding is cleaved by substrates (5) and (6). Substrate (7) produces additional cuts in α-helix 22 described above. Substrates (5) and (6) also cleave the N-terminal region of α-helix 24 where cuts from substrates (2) and (3) are also observed.

Complexes of other SF1 and SF2 helicases with DNA suggest that the translocating strand spans the cleft between HD1 and HD2. Fragments from substrates (5–7) mapping to the Arch domain indicate that this is also true for SF2B helicases (Figure 3B). The Arch domain is centrally located above the two RecA-like folds. Cleavage sites identified within this domain were mapped on the ceiling of the anticipated channel above the interface between the motor domains. All three substrates cleave the loop leading into β-strand 7, as well as, β-strand 9 leading into α-helix 17, which sits above

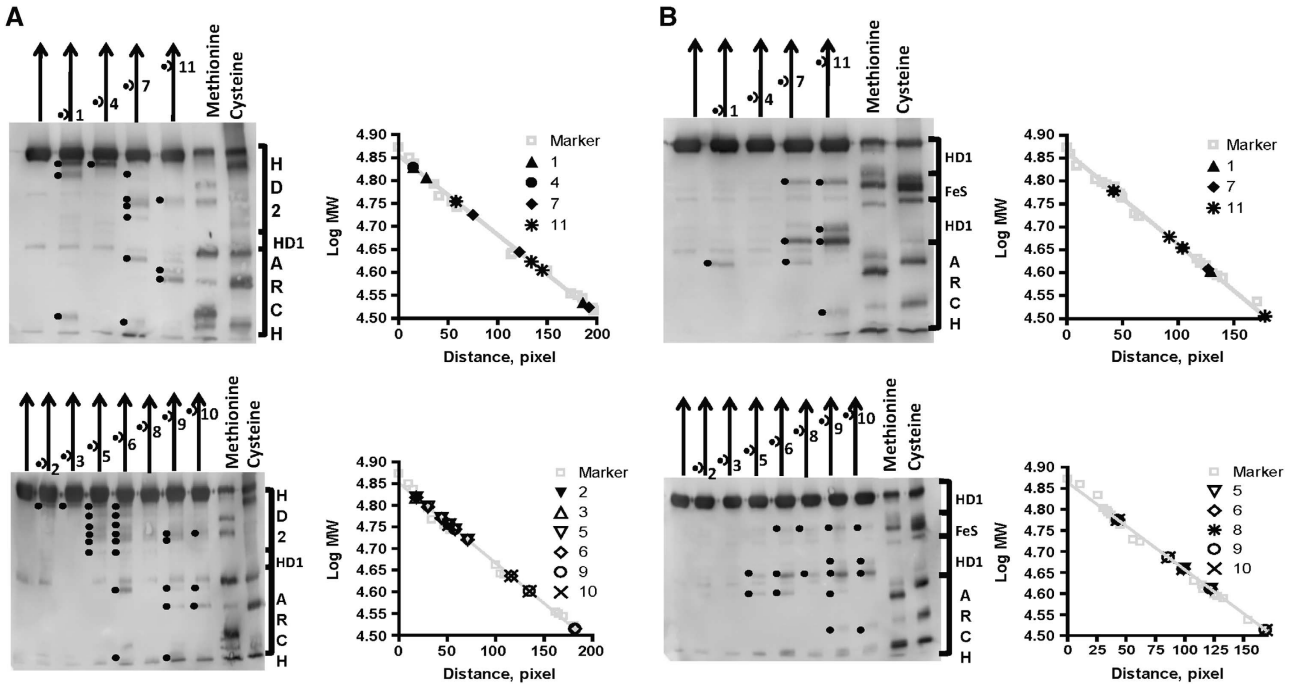

Figure 2 FeBABE generated fragments. Bands were detected by western blot using α-6 × his (N-terminus) antibodies in (**A**) and α-FLAG (C-terminus) antibodies in (**B**). (**A**) α-His (N-terminus) cleavage pattern resulting from FeBABE mediated hydroxyl radical cleavage of XPD. Oligonucleotides containing FeBABE are represented by arrows (5′–3′) positioned above the figures. Positions of FeBABE are indicated by ●) above the gels. Chemical digests of XPD cleaved at methionines and cysteines were used for precise identification of the size for each fragment (●) as determined from migration distance on the gel. The linear relationship of the $\log_{10}$ of the molecular weight of known fragments from the chemical digests was fitted with a straight line and cleavage fragments are indicated. (**B**) α-Flag (C-terminus) cleavage pattern resulting from FeBABE mediated hydroxyl radical cleavage and the chemical digests used to determine the molecular weights of each indicated fragment.

the central channel. Finally, the three substrates also cleave α-helix 12 above the central channel for DNA adjacent to HD1.

The FeS domain is an insertion within HD1 stabilized by the presence of an 4Fe-4S cluster (Rudolf *et al*, 2006; Fan *et al*, 2008; Liu *et al*, 2008; Wolski *et al*, 2008). Two cuts, one generated by substrate (6) and the other by substrate (7) both map to α-helix 5 in the FeS domain (Figure 3B). This helix is located on the entrance side of the central pore formed between the Arch domain, FeS domain and HD1. One of the conserved cysteines (Cys^{113}) essential for the FeS cluster integrity and therefore for translocation is located within this helix.

FeBABE positioned at the 3′-end of DNA (substrates 8–11) yields fewer cuts in HD2 and more cuts in the FeS domain and HD1 (Figure 3C). Cuts in HD2 map to α-helix 20 and the loop leading into α-helix 20. Cuts mapped to the Arch domain appear in the loop above HD2 between α-helix 13 and β-strand 7. α-Helix 12 is cleaved by all four substrates containing FeBABE close to the 3′-end. This helix sits above the central ssDNA binding channel and forms a part of the central pore through which the translocating strand exits the helicase motor domains as the helicase translocates in the 5′ direction. On the other side of the central pore, the N-terminal loop leading into α-helix16 and α-helix16 itself is cleaved by substrates (9–11). Substrates (9–11) also generated two cleavage sites mapped to HD1 (Figure 3C). These cuts were in β-sheet 5 leading into α-helix 11 containing the DEAH residues of the conserved helicase motif II. All four of the 3′-end labelled substrates cleaved α-helix 5 as the 3′-end passes through the central pore as described above for substrates (5–7).

In summary, FeBABE footprinting indicates that XPD binds to ssDNA with the same orientation as SF1 and SF2A helicases. HD2 interacts with the 5′-end of DNA while HD1 interacts with the 3′-end. The large number of fragments generated in HD2 when FeBABE was moved towards the 3′-end of DNA is consistent with the mechanism whereby XPD binding to ssDNA is initiated at the 5′-end of occluded region through recognition by residues in HD2. This allows ssDNA to bind in a number of different registers, which can result in a free and floppy 3′-end capable of generating fragments in all domains of the helicase.

Fluorescence footprinting confirms orientation of XPD on ssDNA

To confirm the results of the FeBABE cleavage experiments, we took advantage of our previously reported observation that the FeS cluster of XPD helicase quenches fluorescent dyes and that the magnitude of fluorescence quenching decreases with distance between the dye and the FeS cluster (Honda *et al*, 2009). We expected that the polarity of bound ssDNA will be reflected in the quenching trend of the Cy5 dye site specifically incorporated into ssDNA substrates. Binding titrations revealed that the total magnitude of quenching measured over the course of the reactions increased as the Cy5 fluorophore was placed closer to the 3′-end compared with the substrates containing fluorophore closer to the 5′-end (Figure 4). Binding curves (Figure 4A) obtained when Cy5 was positioned at either the 5′ or 3′ terminus closely resemble single site binding curves, whereas binding of XPD to centrally positioned Cy5-labelled oligonucleotides appeared more complex. It is possible that at high protein

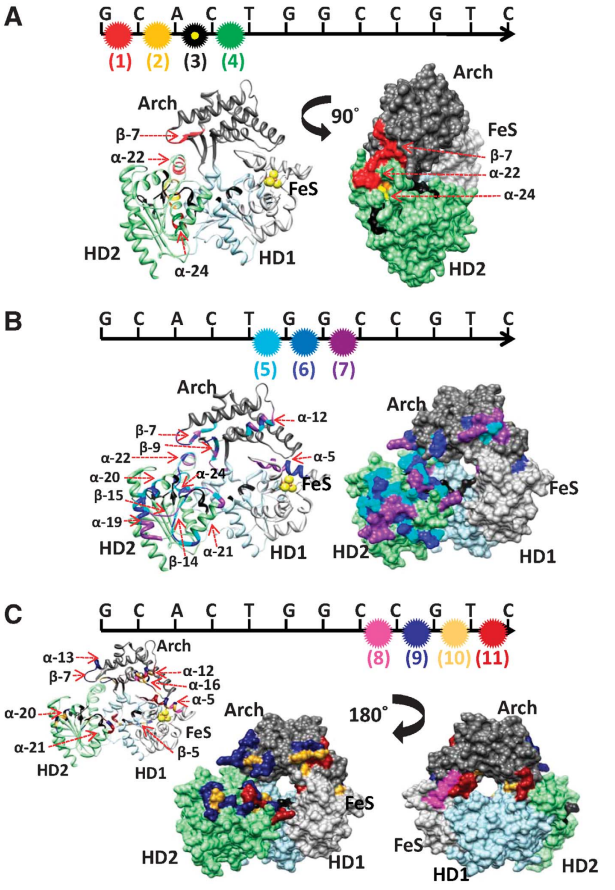

Figure 3 FeBABE generated fragments mapped to XPD. Positions of FeBABE within each set of oligonucleotides are indicated by colour coded asterisks and numbers. Fragments are colour coded with the position of FeBABE from which they were generated as they are mapped on the structure of *Tac*XPD helicase (pdb: 2VSF). Helicase motifs involved in binding to DNA are indicated in black. HD1 appears in light blue. HD2 is coloured light green. The Arch domain appears in dark grey and the FeS domain appears in light grey. (**A**) Fragments generated from FeBABE incorporated at the 5′-end of the substrate. (**B**) Fragments mapped from centrally located FeBABE substrates. (**C**) Fragments mapped on XPD from 3′-end labelled substrates.

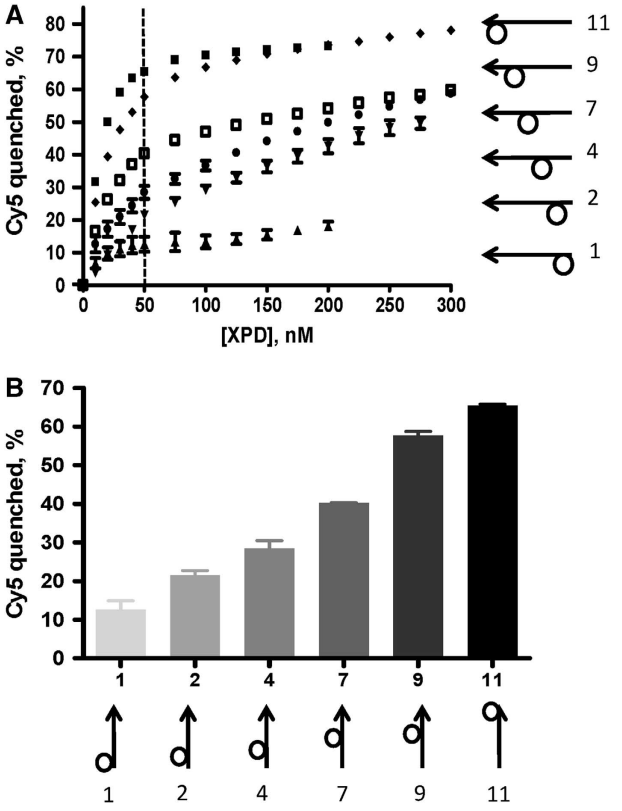

Figure 4 Orientation of XPD binding determined by Cy5 quenching. (**A**) Cy5 was site specifically incorporated into 12mer ssDNA as indicated by open circles on each oligonucleotide. Binding of XPD to six 12mers containing Cy5 at different locations was monitored by following XPD-dependent quenching of Cy5 fluorescence. (**B**) Histogram of the total quenching observed at 50 nM XPD and 10 nM Cy5-labelled ssDNA. Titrations were carried out in duplicate.

concentrations more than one XPD molecule was bound to these substrates resulting in non-saturable quenching. Therefore, the comparisons were made at the XPD concentration (50 nM) corresponding to the inflection point in the binding isotherms. Comparing the data for each substrate obtained in the presence of 50 nM XPD showed that the greatest magnitude of quenching (≈65%) was observed when the Cy5 fluorophore was positioned between nucleotides 11 and 12 at the 3′-end (Figure 4B). Quenching was at its lowest point (≈12%) when Cy5 was incorporated between nucleotides 1 and 2 at the 5′-end (Figure 4B). This confirms the orientation of the helicase revealed by the FeBABE data showing that the 5′-end of DNA is located furthest away from the FeS cluster.

HD1 and the FeS cluster-containing domain contact the translocating strand during duplex unwinding

Given the orientation of XPD when bound to the translocating strand, HD1 and the FeS cluster-containing domain must be at the point of duplex separation, and therefore are expected to contact both the translocating strand and the displaced strand. We hypothesized that a number of positively charged residues and a histidine located on the opposite side of the donut-like hole formed between the HD1, Arch and FeS domains would be responsible for contacting either the displaced strand or the translocating strand (Figure 5). Each of these residues was individually mutated to alanine and subsequently purified to homogeneity (Supplementary Figure S1B). After purification, an FeS cluster was found in all mutants except for C113A which provides one of the required cysteine ligands for the cluster (Supplementary Figure S3A). Purified R88A, K117A and Y130A/F131A mutants have a different shade of colour indicating a compromised FeS cluster (Supplementary Figure S3A). Proper folding of each mutant was confirmed by CD spectroscopy (Supplementary Figure S3B). All purified enzymes were ssDNA-dependent ATPases (Table I). Efficiency of ATP hydrolysis (k_{cat}/K_M) was reduced >20-fold in R88A and C113A mutant enzymes and nearly eight-fold in Y130A/F131A compared with WT (Table I; Supplementary Figure S4A). Binding affinities for both ssDNA and forked DNA were determined using Cy5 quenching as a reporter of bound state for all enzymes except for C113A (which does not contain FeS cluster and therefore does not quench fluorescence) (Table I; Supplementary Figure S4B and C). The binding titrations for K117A and Y130A/F131A resulted in unique curves that may have resulted from the different colour of the enzyme. As a

consequence, binding affinity was determined by fitting the data between 0 and 50 nM or 100 nM XPD as indicated in Table I.

WT enzyme bound ssDNA with $K_D = 13.7$ nM. Several mutant enzymes had altered binding affinity for ssDNA. Affinity of K170A was nearly four-fold lower than that of the wild type, and three-fold lower affinity was observed for K194A. When these two residues were mutated together binding affinity was similar to WT. The triple mutant, K170A/K194A/H198A bound ssDNA nearly 1.5-fold less tightly than the WT.

Binding affinities were determined for each mutant in the absence of sodium chloride for a forked DNA substrate (Table I; Supplementary Figure S4C). WT, R88A, K117A, Y130A, Y130A/F131A and H198A had similar binding affinity (Table I). Approximately, two-fold or more reduction in binding affinity was observed for R116A, F131A, K170A, K194A, K170A/K194A, K170A/H198A, K194A/H198A and K170A/K194A/H198A.

Collectively, these data confirmed that predicted residues do indeed participate in the interaction with DNA.

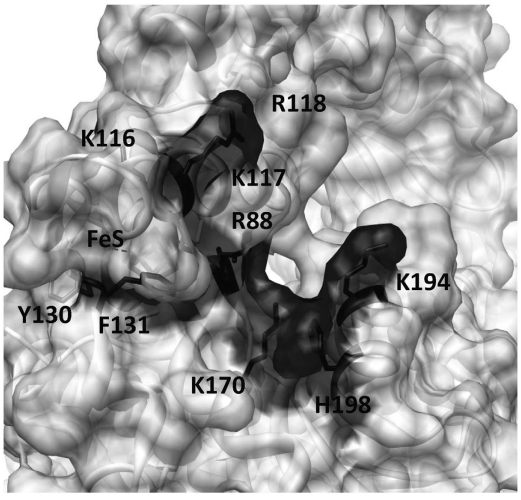

Figure 5 Residues located in the FeS domain and HD1 affect helicase and streptavidin displacement activities of XPD. Surface rendition of FeS, Arch and HD1 domains of XPD. Residues implicated in binding to the translocating strand and involved in duplex separation (black) were replaced with alanine.

Secondary DNA binding site controls force generation, DNA translocation and unwinding by XPD

Translocation, ability to generate force and unwinding activity of mutant XPD enzymes were used to analyse the role of individual residues found in HD1 and the FeS domain of XPD (Figure 6). Translocation and force generation by the wild-type and mutant XPD enzymes were inferred from their ability to facilitate streptavidin displacement from ssDNA oligonucleotide biotinylated near the 3′-end (Morris *et al*, 2001; Pugh *et al*, 2008a). While efficient streptavidin displacement is an established indicator of helicase translocation, the inability to facilitate streptavidin displacement does not necessarily mean that the helicase does not translocate. Therefore, translocation of the selected mutants was also confirmed by following quenching of the DNA-tethered fluorescent dye (Supplementary Figure S6) A complete inability to displace streptavidin, translocate and unwind duplex DNA was observed for the R88A mutant (Figure 6A and B). K117A from the FeS domain is positioned to interact with the translocating strand after initial separation occurs, and it is directed into the pocket towards K170, K194 and H198 (Figure 5). When this residue was replaced with alanine, the mutant was a poorer force generator and subsequently a poorer helicase than the WT enzyme (Figure 6A and B). K117 likely interacts with the translocating strand as it is threaded through the central pore between the Arch, HD1 and FeS domains (Figure 5). Y130A and Y130A/F131A also had lower than WT unwinding ability (Figure 6A). Streptavidin displacement by either Y130A or F131A was similar to the WT enzyme, but when these two residues were simultaneously replaced by alanines, streptavidin displacement decreased two-fold compared with WT (Figure 6B). Individual mutations of three residues K170, K194 and H198 that are located in HD1 and face the groove between HD1 and FeS domain

Table 1 ATPase and binding affinity for XPD and mutants

	ATPase			Binding	
	k_{cat}, s^{-1}	K_M, μM	k_{cat}/K_M, $s^{-1}M^{-1}$	ssDNA K_d, nM	Fork K_d, nM
WT	315 ± 15	235 ± 42	1.34×10^6	13.7 ± 1.6	8.5 ± 2.9
88	65 ± 11	970 ± 392	6.67×10^4	10.2 ± 1.7	9.1 ± 2.6
113	87 ± 27	1357 ± 909	6.42×10^4	ND	ND
116	263 ± 13	184 ± 36	1.43×10^6	13.7 ± 1.6	18.9 ± 3.7
117	200 ± 32	194 ± 122	1.04×10^6	2.8 ± 0.9[a]	11.4 ± 4.7[a]
118	278 ± 13	679 ± 79	4.10×10^6	14.9 ± 1.9	14.9 ± 2.8
130	198 ± 54	820 ± 583	2.42×10^5	11.0 ± 1.4	11.5 ± 3.7
131	183 ± 29	654 ± 285	2.79×10^5	10.6 ± 1.5	17.7 ± 4.1
130/131	140 ± 38	792 ± 568	1.77×10^5	4.7 ± 0.8[a]	9.1 ± 5.2[b]
170	328 ± 42	402 ± 170	8.17×10^5	42.9 ± 3.7	22.6 ± 2.8
194	334 ± 6	290 ± 18	1.15×10^6	31.7 ± 2.8	30.8 ± 3.3
198	322 ± 14	185 ± 31	1.74×10^6	11.5 ± 2.5	4.5 ± 1.7
170/194	301 ± 7	341 ± 26	8.82×10^5	18.3 ± 3.0	21.0 ± 3.4
170/198	336 ± 16	615 ± 77	5.46×10^5	9.5 ± 1.6	29.6 ± 4.1
194/198	276 ± 14	232 ± 39	1.19×10^6	9.6 ± 1.2	21.2 ± 3.7
170/194/198	252 ± 20	596 ± 123	4.23×10^5	19.8 ± 2.4	26.3 ± 3.0

[a]Determined using only the data collected between 0 and 50 nM of XPD.
[b]Determined using only the data collected between 0 and 100 nM of XPD.

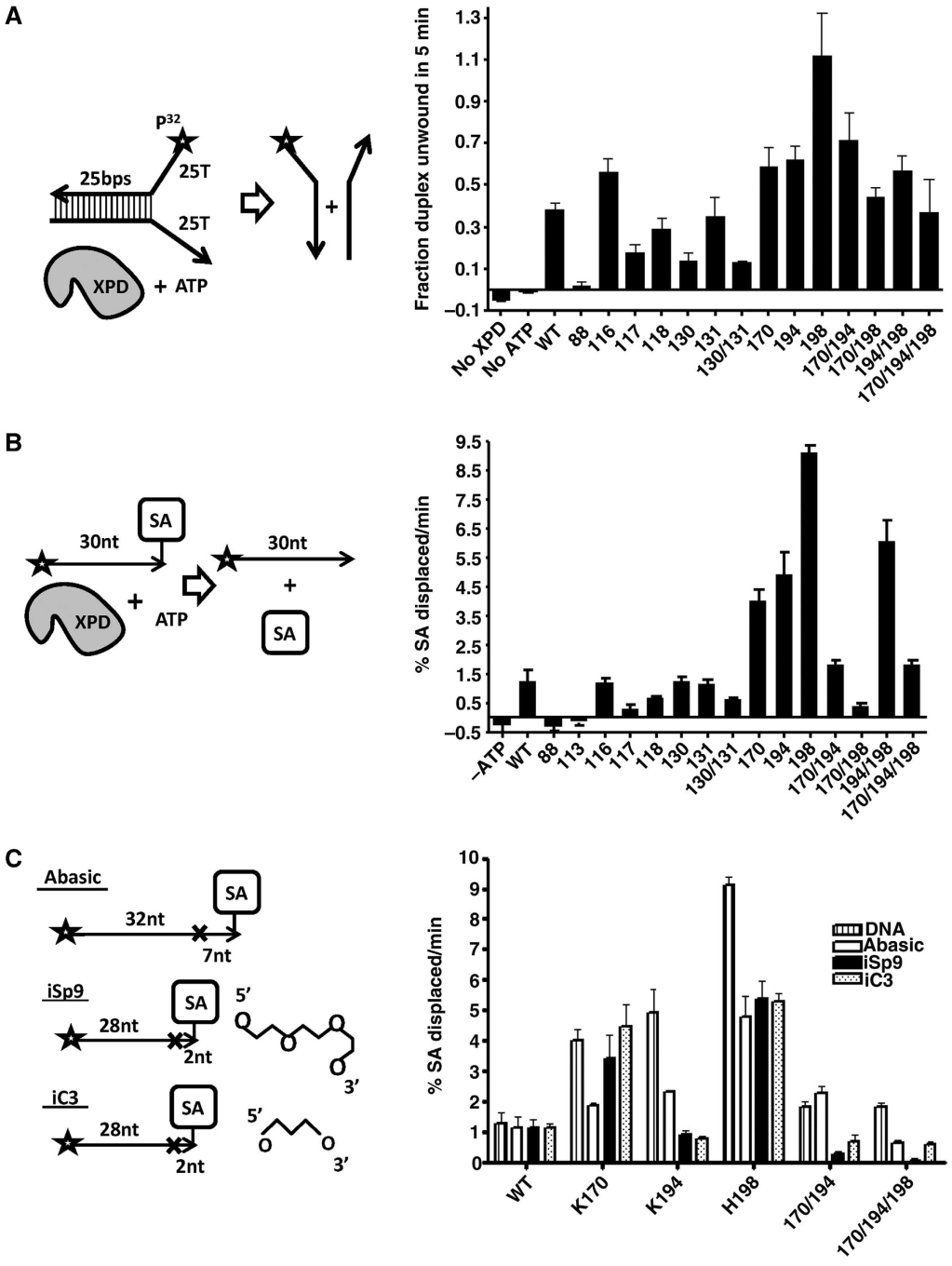

Figure 6 Helicase and motor activities of the wild-type and mutant XPD helicases. (**A**) Histogram displaying results from helicase assays for each mutant analysed. Assays contained 2.5 μM enzyme and 50 nM forked DNA. Reactions were carried out at 45°C. Fraction unwound reflects the ratio of ssDNA product to intact forked duplex after 5 min following initiation with 4 mM ATP. Error bars represent standard deviation from the mean from a minimum of two independent experiments. (**B**) Rate of streptavidin displacement on 10 nM unmodified oligonucleotide by 500 nM of each mutant enzyme at RT. Biotinylated DNA was incubated for 5 min at RT with the enzyme. Translocation was initiated with 3 mM ATP and time points were taken from 0 to 10 min. Error bars represent standard deviation from the mean from a minimum of two independent experiments. (**C**) Rate of streptavidin displacement from modified oligonucleotides. Reactions were carried out as described for (**B**) but using modified oligonucleotides depicted on the left. Error bars represent standard deviation from the mean from a minimum of two independent experiments. X marks the position the modification within each oligo. Abasic oligo lacks a nucleotide at this position. The structures of the backbone modifications are cartooned. Total streptavidin displacement for each oligo and mutant is detailed in Supplementary Figure S5.

demonstrated increased streptavidin displacement and increased helicase activity compared with wild type (Figure 6A and B). H198A mutant was also the fastest and most processive translocase (Supplementary Figure S6). When these residues were mutated in combination with each other, the K170A/K194A mutant still displayed increased unwinding and streptavidin displacement compared with WT, but reduced streptavidin displacement and no difference in unwinding activity when compared with either the K170A or K194A single mutants (Figure 6A and B). The K170A/

H198A mutant had near WT helicase activity and lower streptavidin displacement than WT, and a great reduction in activity compared with the H198A mutant alone (Figure 6A and B). When K194 and H198 were mutated together, streptavidin displacement and helicase activity remained greater than WT (Figure 6A and B). Activity was similar to the K194A mutant alone but greatly reduced compared with H198A. When all three residues were replaced with alanines, the enzyme displayed WT levels of streptavidin displacement and unwinding activities (Figure 6A and B). Unwinding and streptavidin displacement data for these enzymes suggest that these residues form contacts with the translocating strand ahead of the motor core.

Streptavidin displacement from modified oligonucleotides

Modified oligonucleotides containing an abasic site and two different backbone modifications were used to further probe the role of residues K170, K194 and H198 in translocation (Table II; Figure 6C; Supplementary Figure S5). The WT enzyme showed little difference in the ability to displace streptavidin on any of the modified oligos compared with unmodified DNA (Table II; Figure 6C; Supplementary Figure S5). K170A had increased ability to displace streptavidin on DNA compared with WT and was unaffected by either of the backbone modifications. K170A was slowed only by the abasic site to the same rate of streptavidin displacement as the WT enzyme. K194A displaced streptavidin four-fold faster on normal DNA than WT, but was slowed by all three of the modified oligonucleotides with the greatest effect seen with the backbone modifications. H198A was slowed by all three modifications compared with unmodified DNA. However, this enzyme still translocated three-fold faster on the abasic oligo, ten-fold faster on the oxygen containing backbone modified oligo (isp9) and five-fold faster on the carbon only backbone modified oligonucleotide (iC3). K170A/K194A mutant had slightly elevated rate of streptavidin displacement on DNA and abasic DNA, but was inhibited 2.5-fold by the isp9 modification and showed no deviation from WT on iC3 modified oligonucleotide. When all three residues were replaced by alanine, the rate of streptavidin displacement was similar to WT for DNA, two-fold lower on abasic DNA, 14-fold lower on isp9 and two-fold lower on iC3 backbone modifications.

FeS domain contains a wedge-like feature

Our previous data implicated the FeS domain as being the point of duplex separation in XPD helicase (Pugh *et al*, 2008a). If the groove containing K170, K194 and H198 indeed interacts with translocating strand, the site of the duplex separation should be upstream of this groove. *Tac*XPD contains two aromatic residues Y130 and F131 poised to base stack with DNA from the duplex as strand separation occurs (Figure 5). F131 would stack with the translocating strand as it is directed into the central pore by K170, K194, H198 and R88. Y130 is oriented opposite of F131 and may interact with the displaced strand. To test whether Y130 and F131 act as a separation point for the duplex, each residue was replaced with alanine. When either residue was replaced individually no change in streptavidin displacement was observed (Figure 6B). Together, a decrease in streptavidin displacement was observed (Figure 6B). No change in helicase activity was observed for F131A, however, both the Y130A, and double mutant, Y130A/F131A displayed reduced unwinding activity, suggesting that Y130 plays a role in positioning of the displaced strand during unwinding (Figure 6A). The attenuated helicase activity by Y130A is in line with previous data, in which XPD is a much poorer helicase when acting on a 5′ partial duplex substrate compared with a forked substrate (Pugh *et al*, 2008a). This confirms that positioning of the displaced strand is important for positioning and orienting XPD for unwinding.

Discussion

Previous biochemical and structural studies by us (Pugh *et al*, 2008a, b; Honda *et al*, 2009) and others (Rudolf *et al*, 2006; Fan *et al*, 2008; Liu *et al*, 2008) suggested two mutually exclusive mechanistic explanations for selection of translocation polarity in SF2 helicases. Although most of the existing data were consistent with either model, the results of our fluorescence quenching studies somewhat favored a model whereby 5′–3′ translocating XPD helicase binds ssDNA with the same orientation as SF1A, SF1B and SF2A helicases. In 2008, the crystal structures of XPD from three different archaea provided the first structural insights into an SF2B helicase (Fan *et al*, 2008; Liu *et al*, 2008; Wolski *et al*, 2008). All three groups proposed that the translocating strand is threaded through a central pore formed by the Arch, FeS domains and HD1 (Figures 5 and 7). This requires duplex separation to occur on one side of the helicase prior it reaching the hole. Two possible sites of duplex separation were proposed, the FeS cluster-containing domain (Fan *et al*, 2008; Liu *et al*, 2008; Pugh *et al*, 2008a) and a wedge-like structure in HD2 (Wolski *et al*, 2008) reflecting two possible binding orientations of XPD helicase. Here, using the FeBABE reverse footprinting technique, we determined the orientation of the XPD helicase when bound to ssDNA. Our data indicate that SF2B helicases bind to the translocating strand with the same orientation as SF1 and SF2A helicases (Figure 7). HD2 contacts the 5′-end of the translocating strand and the 3′-end interacts with HD1. This appears to be a shared characteristic for SF1 and SF2 helicases, and is further evidenced by the first binary complex of an SF2B helicase bound to a short ssDNA fragment, which is reported in the accompanying manuscript (Kuper *et al*, 2011).

Table 2 Rate of streptavidin displacement (% streptavidin displaced per minute)

	WT	K170A	K194A	H198A	K170A/K194	K170A/K194A/H198A
DNA	1.26 ± 0.39	4.01 ± 0.38	4.91 ± 0.79	9.09 ± 0.27	1.84 ± 0.16	1.81 ± 0.17
Abasic	1.16 ± 0.34	1.87 ± 0.08	2.32 ± 0.06	4.77 ± 0.71	2.27 ± 0.21	0.64 ± 0.08
iSp9	1.13 ± 0.27	3.41 ± 0.78	0.93 ± 0.12	5.36 ± 0.63	0.27 ± 0.08	0.06 ± 0.08
iC3	1.16 ± 0.11	4.46 ± 0.73	0.78 ± 0.09	5.29 ± 0.25	0.67 ± 0.21	0.59 ± 0.08

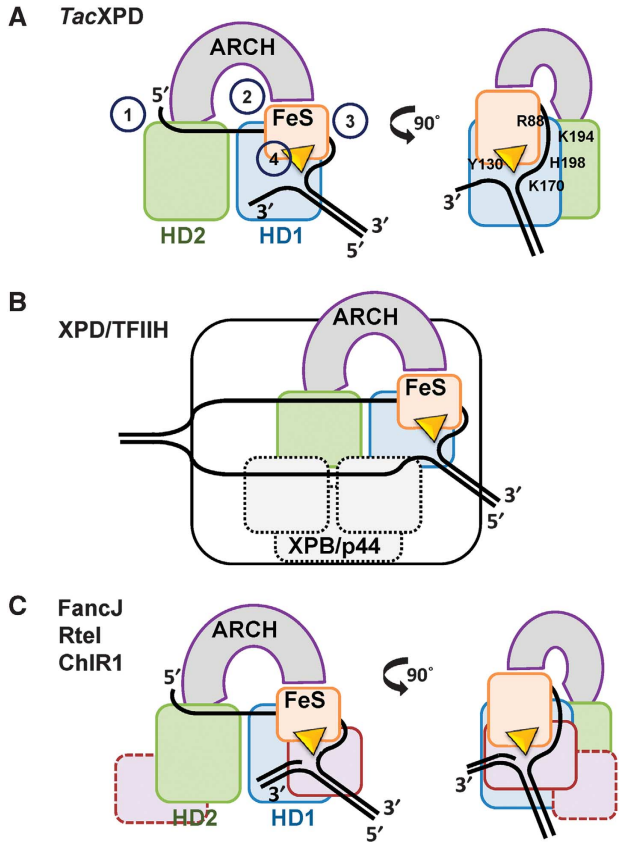

Figure 7 Model for duplex unwinding by SF2B helicases. (**A**) Model of *Tac*XPD bound to a forked DNA substrate with DNA interaction positions identified. (1) Represents the initial binding or recognition point in HD2. (2) DNA passes through the central pore formed between the Arch, FeS and HD1 domains. (3) DNA binding region specific for Rad3 helicases formed by residues from HD1 and the FeS domains. (4) Proposed wedge and point of duplex separation. (**B**) Depiction of XPD as part of the TFIIH complex during transcription and nucleotide excision repair. (**C**) Extension of our binding model based upon *Tac*XPD to other SF2B helicases, FancJ, Rtel and ChlR1. Insertions conferring substrate specificity for branched DNA substrates are outlined in red. Interaction between DNA substrates and these insertions may also be responsible for higher helicase rates and processivities typically observed in these helicases.

A significant difference revealed in binary complexes of SF1 and SF2 helicases and DNA lies in critical contacts between the helicase and the translocating strand. For SF1A helicases, such as PcrA and UvrD, the helicase interacts primarily with the bases of the oligonucleotide including critical base stacking and flipping as the helicase moves along its substrate (Velankar *et al*, 1999). Structural data for the SF1B helicase, RecD (Saikrishnan *et al*, 2009), and SF2A helicases, Hel308 (Buttner *et al*, 2007) and NS3 (Kim *et al*, 1998), indicate that these helicases interact primarily with the phosphodiester backbone of DNA during translocation. With exception of the accompanying manuscript, no structural information regarding interaction between XPD or related SF2B helicases with DNA is available, however, numerous biochemical studies suggest that these enzymes interact with the phosphodiester backbone of the translocating strand similarly to SF2A and SF1B helicases and differ from SF1A enzymes that interact with bases of the bound nucleic acid. XPD readily translocates past base modifications such as bulky extrahelical modifications and abasic sites (Rudolf *et al*, 2010; Figure 6C). Moreover, it can bypass a ssDNA binding protein, RPA2, without displacing it (Honda *et al*, 2009), strongly suggesting that translocation by XPD involves critical contacts with the DNA backbone similarly to SF1B and SF2A helicases. A specific type of UV induced lesion, cyclobutane pyrimidine dimers (CPDs), prevents translocation by XPD when positioned in the translocating strand (Mathieu *et al*, 2010). This type of lesion may interfere with the enzyme's ability to interact with the translocating strand through residues K170, K194 and H198.

Based on the results of our FeBABE experiments, we expected duplex separation to occur somewhere between HD1 and the FeS domain. We hypothesized that two aromatic residues in the FeS domain oriented in opposite directions positioned to base stack with duplex DNA was the point of duplex separation (Figure 5). The presence of two aromatic residues is highly conserved in the FeS domain of Rad3 helicases (Pugh *et al*, 2008a; Supplementary Figure S7B). They appear one residue removed from the highly conserved third cysteine, which provides one of the ligands to the FeS cluster for most Rad3 helicases (Supplementary Figure S7B). In the structure of XPD from *S. acidocaldarius*, these two residues appear in a similar position and orientation as the aromatic residues in *Tac*XPD (Supplementary Figure S7A; Fan *et al*, 2008). In a sequence alignment, these residues can be found flanking the fourth conserved cysteine contributing a required ligand to the FeS cluster (Supplementary Figure S7B). When F131 is replaced with alanine no noticeable effect on streptavidin displacement or unwinding activity is observed (Figure 6A and B). In the accompanying manuscript, Kuper *et al* suggest that F133 whose mutation displays decreased binding affinity for ssDNA without affecting unwinding activity, contributes to the wedge (Kuper *et al*), and therefore might be functionally redundant with F131.

The orientation of XPD bound to DNA and the position of these two aromatic residues indicate they would be the first to interact with damaged DNA bases to be repaired through NER as XPD translocates along DNA. Not surprisingly, XPD stalls upon encountering CPDs on the translocated strand (Mathieu *et al*, 2010). Upon encountering, a CPD on the displaced strand XPD dissociates (Mathieu *et al*, 2010). These two observations imply two different sensory mechanisms employed by XPD through conserved residues in its FeS domain. A base modification sensing role for F131 likely would not interfere with translocation by XPD. Other mammalian Rad3 helicases (FancJ, Rtel and ChlR1) contain additional insertions in the HD1, which may not only confer distinct substrate specificities, but also a different DNA damage sensing mechanism.

A number of positively charged residues in the FeS domain and HD1 and a histidine located in HD1 were mutated to alanine to determine if there was any effect on helicase activity that would suggest they interact with the translocating strand. One residue of note R88 sits centrally in the pore where DNA is presumed to pass through. While the R88A mutant was purified with an FeS cluster, the integrity of the 4Fe-4S cluster may have been compromised as indicated by the different absorbance spectra and colour (Supplementary Figures S1 and S3A). R88A mutant appears to be properly folded (Supplementary Figure S3B and C). It displayed de-

creased ATP hydrolysis activity (Table I; Supplementary Figure S4A) and was completely defective in translocation and helicase activity (Figure 6A and B). R88 is the equivalent of R112 in human XPD which when mutated to a histidine results in an inactive helicase and causes trichothiodystrophy as a consequence of defective NER (Dubaele *et al*, 2003; Nishiwaki *et al*, 2004, 2008). Despite the loss of the ability to displace streptavidin and helicase activity, the R88A mutant bound to ssDNA and forked DNA with the same affinity as the wild-type enzyme (Table I). Our R88A enzyme retained a form of an FeS cluster following purification, in contrast to the R112H variant in *S. acidocaldarius* (K84H) which lost its cluster upon purification (Rudolf *et al*, 2006). In the structure presented in the accompanying manuscript (Kuper *et al*, 2011), R88 participates in coordination of the sulphate ion, which has likely taken a place occupied in the XPD–DNA complex by phosphodiester backbone of translocating strand. R88, therefore, provides a bridge between FeS cluster and DNA.

A triad of residues, K170, K194 and H198 lie next to R88 and can be seen in line with the central pore (Figure 5). Individual replacement of each of these residues for alanine resulted in increased streptavidin displacement and helicase activity (Figure 6A and B). We propose that K170 and H198 interact with DNA bases and K194 form contacts with the phosphate backbone and serve to thread DNA through the central pore in XPD as it translocates along ssDNA. H198 appears to inhibit the helicase through base interactions and may be responsible for generating force as the helicase translocates. Residues K170 and K194 appear to overpower this inhibition by H198.

The K170 residue is highly conserved in Rad3 helicases with the exception being *S. acidocaldarius* (Supplementary Figure S7). In *S. acidocaldarius*, however, one of the two arginine residues (165 and 163) may play similar functional role (Supplementary Figure S7A). The ability of K170A to translocate on both of the backbone modified oligos but its reduced streptavidin displacement on the abasic oligo suggests that this residue may interact with DNA bases on the translocating strand and may be involved in positioning the base to interact with H198 for regulation. The K194A enzyme was slowed by all three modifications. The largest effect was seen with the backbone modifications, suggesting this residue interacts with the DNA backbone of the translocating strand.

Unwinding by H198A was at least two-fold greater than WT and the rate of streptavidin displacement was nine-fold higher than WT (Figure 6A and B). Additionally, H198A mutant displayed the most vigorous translocase activity (Supplementary Figure S6). This residue may serve as a 'gatekeeper' that regulates helicase activity through a critical base stacking interaction or by donating a hydrogen bond to a hydrogen bond acceptor on the phosphodiester backbone of ssDNA. Eliminating this interaction increases unwinding activity and is consistent with increased helicase activity observed for *Fac*XPD in the presence of the ssDNA binding protein RPA2 (Pugh *et al*, 2008b). When K170, K194 and H198 residues were mutated in combination with each other, unwinding activity by the double mutants was still greater than the WT and when all three were replaced with alanines, unwinding activity returned to the WT level. Moreover, R88, K170, H198 and Y166 coordinate a sulphate ion in the structure of XPD, which likely mimics the position of the phosphate in ssDNA backbone (Kuper *et al*, 2011). Based on these findings, it is apparent that these three residues are involved in directing the translocating strand through the central channel, by gripping it tight enough to maintain binding to the strand, and yet loose enough to be overcome by the energy released through ATP hydrolysis. A residue analogous to H198 can be identified in some other Rad3 helicases including XPD from *F. acidarmanus* and *H. sapiens* Rtel1 (Supplementary Figure S7B). F167 can be found in a similar position in the structure of *S. acidocaldarius* (Supplementary Figure S7A) and may play a gatekeeper function. The lack of a gatekeeper in human and yeast XPD may be due to XPD being a part of the TFIIH complex (Wang *et al*, 1994; Tirode *et al*, 1999; Egly and Coin, 2011; Fuss and Tainer, 2011). For other Rad3 helicases, it is expected that they are faster and more processive helicases than XPD and the lack of gatekeeper may explain this observation.

In summary, we have demonstrated that SF2B helicases bind with the same orientation as SF2A and SF1 helicases (schematically depicted in Figure 7). A wedge-like feature flanking the FeS cluster is a point of duplex separation from which the translocating strand is funneled through the central pore of the helicase into the motor core. It remains to be determined how translocation is achieved by SF2B helicases and how reversal of the conformational change between the motor domains is induced. DNA-interacting residues located at the interface between HD1 and the FeS cluster-containing domain may provide a larger and higher affinity binding site for DNA compared with just the binding site formed by the conserved helicase motifs (Figure 7A). This may also be the source of force generation for translocation. The loss of translocation by R88A suggests that both sides of the pore participate in coupling ATP hydrolysis with translocation through coordinated conformational changes between HD1 and HD2 on one side and HD1, the FeS and the Arch domain on the other side of the pore. The extended binding site and unique structural architecture of SF2B helicases may be the features responsible for 5′–3′ translocation polarity. Our data can be extrapolated to all identified 5′–3′ translocating SF2 helicases, which currently include XPD (Rad3), DinG, FancJ (Bach1), Rtel and ChlR1 enzymes (Figure 7C) based on sequence homology and expected structural and mechanistic similarity (White, 2009; Wu *et al*, 2009).

Materials and methods

T. acidophilum XPD and mutants

The open reading frame for *T. acidophilum* XPD helicase was amplified using genomic DNA (purchased from ATCC) and primers shown in Supplementary Table S2. For incorporation of the Flag tag on the C-terminus of XPD, the nucleotide sequence encoding the Flag peptide (GDYKDDDK) was cloned into pET28a using *Nde*I and *Xho*I restriction enzymes sites. QuickChange II XL Site-Directed Mutagenesis Kit and QuickChange Lightning Site-directed Mutagenesis Kit (Stratagene) and primers shown in Supplementary Table S2 were used to produce the mutant constructs.

Expression and purification of TacXPD and mutants

*Tac*XPD and all mutants were overexpressed in Rosetta (DE3) plysS (Invitrogen) and purified as described in Pugh *et al* (2008a) for *Fac*XPD. Concentration of the purified *Tac*XPD was determined spectrophotometrically using $\varepsilon_{280} = 66380\,M^{-1}\,cm^{-1}$ or $\varepsilon_{280} = 64890\,M^{-1}\,cm^{-1}$ for tyrosine to alanine mutants.

Labelling of oligonucleotides with FeBABE

Positions of phosphorothioate linkers at specific locations in each oligonucleotide are indicated in the figures. Oligonucleotides were

modified with FeBABE in 30 μl buffer containing 20 mM MOPS (pH 7.0); 2 mM EDTA, 50 μg FeBABE and 50 μM (molecules) ssDNA. Reactions were incubated at 50°C for 3 h. G-25 columns (GE) equilibrated in 50 mM MOPS (pH 8.0); 50 mM NaCl, 10 mM $MgCl_2$, 1 mM EDTA and 15% glycerol, were used to remove unincorporated FeBABE and for buffer exchange. The labelled oligonucleotides were aliquoted and stored at −80°C.

FeBABE mediated protein cleavage reactions

FeBABE cleavage reactions were carried out in 10 μl buffer containing 50 mM MOPS (pH 8.0), 50 mM NaCl, 0.1 mM EDTA, 10 mM $MgCl_2$, 10% glycerol and 7 μM *Tac*XPD. In all, 4 μl of 25 μM FeBABE labelled duplex substrate (7 μM final) was added to each reaction and incubated at RT for 10 min. Cleavage was initiated by adding 1 μl of 50 mM ascorbic acid and 10 mM EDTA (5 mM ascorbic acid and 1 mM EDTA final) immediately followed by 1 μl of freshly prepared 50 mM H_2O_2 and 10 mM EDTA (5 mM H_2O_2 and 1 mM EDTA final). The reaction was then vortexed for 5 s, given a pulse spin and incubated at RT for 30 s. The reactions were quenched by the addition of 6 μl of 6 × SDS sample loading buffer (60% glycerol, 300 mM Tris–HCl (pH 6.8) 12% SDS, 10% β-mercaptoethanol, 0.1% bromophenol blue). Reaction mixtures were allowed to incubate at RT for 5 min and boiled for 3 min. Digested proteins were separated by electrophoresis on polyacrylamide gels of the indicated percentage by loading 2.5 μl of sample per lane.

Chemical digests of TacXPD

Two ladders were created for precise identification of the cleaved fragments produced by FeBABE. *Tac*XPD digested with NTCB which cleaves proteins N-terminal to cysteines was prepared by dialysing 20 μl of 536 μM *Tac*XPD against cleavage buffer (100 mM MOPS 8.5; 8 M urea) for 7 h at 37°C. NTCB was added to a final concentration of 4.5 mM. The reaction was allowed to incubate overnight at 37°C and quenched by addition of 1% (v/v) SDS (final) and 1% (v/v) β-mercaptoethanol (final).

*Tac*XPD digest with CNBr which cleaves C-terminal to methionines was prepared by incubating in 1.5% SDS (50 μl) for 30 min at 65°C followed by the addition of 40 mM HCl (final) and 40 mM CNBr (final). Digests were allowed to proceed for 10 min at 65°C and quenched by addition of 8 μl 6 × SDS sample loading buffer (60% glycerol, 300 mM Tris–HCl (pH 6.8) 12% SDS, 10% β-mercaptoethanol, 0.1% bromophenol blue) and 8 μl 1 M triethanolamine HCl (pH 9.0).

Identification of the protein fragments in western blots

Proteins were transferred onto PVDF membranes and detected by primary antibodies (mouse, α-his and α-flag) followed by the secondary antibody rabbit, α-mouse conjugated to alkaline phosphatase. The membranes were incubated with ECF substrate (GE) and visualized using a STORM Phosphorimager (GE).

Fragment analysis

Images were analysed using ImageQuant 5.2. Analysis was performed by drawing a line vertically from the top of each lane to the bottom. The lines were all adjusted to the same height. All lines were selected and a graph was created based on band intensity (y) and migration distance in pixels (x). The migration distance for each fragment was measured and recorded.

The chemical digests of *Tac*XPD provided a molecular ruler. The $\log_{10}$ of the molecular weight for each fragment was plotted as function of migration distance in pixels using GraphPad Prism and fitted to the first order polynomial (straight line). Molecular weights for each FeBABE cleavage fragment were determined by measuring the migration distance, obtaining the $\log_{10}$ value from the straight line fit of the molecular ruler, and taking the inverse log (10^n).

Residue number for each fragment was estimated using the 'Protein Parameters' program with Expasy proteomics tools webpage (http://ca.expasy.org/tools/protparam.html). A summary of fragments can be found in Supplementary Table S1.

Images

Molecular graphics images were produced using the UCSF Chimera package from the Resource for Biocomputing, Visualization, and Informatics at the University of California, San Francisco (supported by NIH P41 RR-01081; Pettersen *et al*, 2004).

Cy5 fluorescence quenching binding assays

XPD binding to Cy5-labelled ssDNA was monitored as previously described (Pugh *et al*, 2008a, b). Titration reactions were carried out in duplicate with 10 nM Cy5-labelled DNA at 25°C. The duplex forked structure used in determining affinity of XPD for the forked structure was annealed as described in Pugh *et al* (2008a). Titrations were carried out in duplicate or triplicate as described in Pugh *et al* (2008a) in 20 mM MES (pH 6.5).

ATPase assays

ATPase assays were carried out using a continuous spectrophotometric assay (Kreuzer and Jongeneel, 1983) as described previously (Pugh *et al*, 2008a) in buffer containing 20 mM MES (pH 6.5), 5 mM $MgCl_2$, 1 mM DTT, 45–70 units per ml of pyruvate kinase, 30–50 units per ml of lactic dehydrogenase, 0.2 mg ml^{-1} NADH, 2 mM phosphoenolpyruvate, 10 μM (nucleotides) poly(dT) and 50 nM enzyme. ATP was titrated into individual reactions from 0 to 3 mM.

Helicase assays

Unwinding by XPD and mutant enzymes was monitored using gel-based helicase assays as described in Wolski *et al* (2008) with the following exceptions. Each reaction (40 μl) contained 50 nM forked DNA substrate, and 2.5 μM XPD.

Circular dichroism spectroscopy

Overall folding of the enzymes was assessed by CD spectroscopy as described previously (Pugh *et al*, 2008a). Thermal denaturation experiments were performed with 2 μM TacXPD in 50 mM boric acid (pH 8.0), 100 mM KCl, 1 mM DTT. The temperature of the cuvette was controlled using a circulating water bath. Ten spectra were collected and averaged at each temperature from 260 to 190 nm. The ellipticity at 220 nm as a function of temperature was plotted and fit to a two-state reversible folding model.

Streptavidin displacement assays

Streptavidin displacement was used to monitor translocation by XPD and various mutants on DNA and modified oligonucleotides as described previously (Pugh *et al*, 2008a) with the following exceptions. The buffer contained 20 mM MES (pH 6.5) and the reactions used 500 nM *Tac*XPD. Streptavidin displacement was initiated by the addition of 3 mM ATP.

Stopped-flow fluorescence translocation assay

Translocation experiments were performed using a SX20 stopped-flow apparatus at 65°C (Applied Photophysics Ltd., Leatherhead, UK). In all, 200 nM TacXPD (or $TacXPD^{H198A}$) was preincubated with 200 nM of Cy3-labelled ssDNA substrate 42mer-5′-Cy3 (Supplementary Table S2) in 20 mM MES (pH 6.5). The protein–DNA mixture was loaded into one syringe of the stopped-flow apparatus. Translocation reactions were initiated by rapid 1:1 mixing with 5 mM ATP and 10 mM $MgCl_2$ (in MES). Final solution conditions were therefore 100 nM TacXPD, 100 nM DNA, 2.5 mM ATP and 5 mM $MgCl_2$. Cy3 fluorophore was excited at 515 nm and its emission was monitored at all wavelengths >570 nm using a cutoff filter (Applied Photophysics).

Supplementary data

Supplementary data are available at *The EMBO Journal* Online (http://www.embojournal.org).

Acknowledgements

We thank Dr Caroline Kisker and Dr Jochen Kuper for sharing their data prior to publication, Dr Masayoshi Honda and Shyamal Subramanyam for critically reading the manuscript. This work was supported by HHMI Early Career Scientist Award to MS. CGW is an American Cancer Society postdoctoral scholar.

Author contributions: RAP, CGW and MS designed the study; RAP and CGW performed the experiments and data analysis; RAP, CGW and MS interpreted the data and wrote the manuscript.

Conflict of interest

The authors declare that they have no conflict of interest.

References

Buttner K, Nehring S, Hopfner KP (2007) Structural basis for DNA duplex separation by a superfamily-2 helicase. *Nat Struct Mol Biol* **14:** 647–652

Coin F, Oksenych V, Egly JM (2007) Distinct roles for the XPB/p52 and XPD/p44 subcomplexes of TFIIH in damaged DNA opening during nucleotide excision repair. *Mol Cell* **26:** 245–256

Dubaele S, Proietti De Santis L, Bienstock RJ, Keriel A, Stefanini M, Van Houten B, Egly JM (2003) Basal transcription defect discriminates between xeroderma pigmentosum and trichothiodystrophy in XPD patients. *Mol Cell* **11:** 1635–1646

Egly J-M, Coin F (2011) A history of TFIIH: two decades of molecular biology on a pivotal transcription/repair factor. *DNA Repair* **10:** 714–721

Fairman-Williams ME, Guenther UP, Jankowsky E (2010) SF1 and SF2 helicases: family matters. *Curr Opin Struct Biol* **20:** 313–324

Fan L, Fuss JO, Cheng QJ, Arvai AS, Hammel M, Roberts VA, Cooper PK, Tainer JA (2008) XPD helicase structures and activities: insights into the cancer and aging phenotypes from XPD mutations. *Cell* **133:** 789–800

Fuss JO, Tainer JA (2011) XPB and XPD helicases in TFIIH orchestrate DNA duplex opening and damage verification to coordinate repair with transcription and cell cycle via CAK kinase. *DNA Repair* **10:** 697–713

Honda M, Park J, Pugh RA, Ha T, Spies M (2009) Single-molecule analysis reveals differential effect of ssDNA-binding proteins on DNA translocation by XPD helicase. *Mol Cell* **35:** 694–703

Kim JL, Morgenstern KA, Griffith JP, Dwyer MD, Thomson JA, Murcko MA, Lin C, Caron PR (1998) Hepatitis C virus NS3 RNA helicase domain with a bound oligonucleotide: the crystal structure provides insights into the mode of unwinding. *Structure* **6:** 89–100

Kreuzer KN, Jongeneel CV (1983) Escherichia coli phage T4 topoisomerase. *Methods Enzymol* **100:** 144–160

Kuper J, Wolski SC, Michels G, Kisker C (2011) Functional and structural studies of the nucleotide excision repair helicase XPD suggest a polarity for DNA translocation. *EMBO J* (advance online publication, 11 November 2011; doi:10.1038/emboj.2011.374)

Liu H, Rudolf J, Johnson KA, McMahon SA, Oke M, Carter L, McRobbie AM, Brown SE, Naismith JH, White MF (2008) Structure of the DNA repair helicase XPD. *Cell* **133:** 801–812

Luo D, Xu T, Watson RP, Scherer-Becker D, Sampath A, Jahnke W, Yeong SS, Wang CH, Lim SP, Strongin A, Vasudevan SG, Lescar J (2008) Insights into RNA unwinding and ATP hydrolysis by the flavivirus NS3 protein. *EMBO J* **27:** 3209–3219

Mathieu N, Kaczmarek N, Naegeli H (2010) Strand- and site-specific DNA lesion demarcation by the xeroderma pigmentosum group D helicase. *Proc Natl Acad Sci USA* **107:** 17545–17550

Meares CF, Datwyler SA, Schmidt BD, Owens J, Ishihama A (2003) Principles and methods of affinity cleavage in studying transcription. *Methods Enzymol* **371:** 82–106

Morris PD, Tackett AJ, Raney KD (2001) Biotin-streptavidin-labeled oligonucleotides as probes of helicase mechanisms. *Methods* **23:** 149–159

Nishiwaki T, Kobayashi N, Iwamoto T, Yamamoto A, Sugiura S, Liu YC, Sarasin A, Okahashi Y, Hirano M, Ueno S, Mori T (2008) Comparative study of nucleotide excision repair defects between XPD-mutated fibroblasts derived from trichothiodystrophy and xeroderma pigmentosum patients. *DNA Repair (Amst)* **7:** 1990–1998

Nishiwaki Y, Kobayashi N, Imoto K, Iwamoto TA, Yamamoto A, Katsumi S, Shirai T, Sugiura S, Nakamura Y, Sarasin A, Miyagawa S, Mori T (2004) Trichothiodystrophy fibroblasts are deficient in the repair of ultraviolet-induced cyclobutane pyrimidine dimers and (6-4)photoproducts. *J Invest Dermatol* **122:** 526–532

Owens JT, Miyake R, Murakami K, Chmura AJ, Fujita N, Ishihama A, Meares CF (1998) Mapping the sigma70 subunit contact sites on Escherichia coli RNA polymerase with a sigma70-conjugated chemical protease. *Proc Natl Acad Sci* **95:** 6021–6026

Pettersen EF, Goddard TD, Huang CC, Couch GS, Greenblatt DM, Meng EC, Ferrin TE (2004) UCSF Chimera—a visualization system for exploratory research and analysis. *J Comput Chem* **25:** 1605–1612

Pugh RA, Honda M, Leesley H, Thomas A, Lin Y, Nilges MJ, Cann IK, Spies M (2008a) The iron-containing domain is essential in Rad3 helicases for coupling of ATP hydrolysis to DNA translocation and for targeting the helicase to the single-stranded DNA-double-stranded DNA junction. *J Biol Chem* **283:** 1732–1743

Pugh RA, Lin Y, Eller C, Leesley H, Cann IK, Spies M (2008b) Ferroplasma acidarmanus RPA2 facilitates efficient unwinding of forked DNA substrates by monomers of FacXPD helicase. *J Mol Biol* **383:** 982–998

Pyle AM (2008) Translocation and unwinding mechanisms of RNA and DNA helicases. *Annu Rev Biophys* **37:** 317–336

Rudolf J, Makrantoni V, Ingledew WJ, Stark MJ, White MF (2006) The DNA repair helicases XPD and FancJ have essential iron-sulfur domains. *Mol Cell* **23:** 801–808

Rudolf J, Rouillon C, Schwarz-Linek U, White MF (2010) The helicase XPD unwinds bubble structures and is not stalled by DNA lesions removed by the nucleotide excision repair pathway. *Nucleic Acids Res* **38:** 931–941

Saikrishnan K, Griffiths SP, Cook N, Court R, Wigley DB (2008) DNA binding to RecD: role of the 1B domain in SF1B helicase activity. *EMBO J* **27:** 2222–2229

Saikrishnan K, Powell B, Cook NJ, Webb MR, Wigley DB (2009) Mechanistic basis of 5′-3′ translocation in SF1B helicases. *Cell* **137:** 849–859

Schmidt BD, Meares CF (2002) Proteolytic DNA for mapping protein-DNA interactions. *Biochemistry* **41:** 4186–4192

Singleton MR, Dillingham MS, Gaudier M, Kowalczykowski SC, Wigley DB (2004) Crystal structure of RecBCD enzyme reveals a machine for processing DNA breaks. *Nature* **432:** 187–193

Singleton MR, Dillingham MS, Wigley DB (2007) Structure and mechanism of helicases and nucleic acid translocases. *Annu Rev Biochem* **76:** 23–50

Soultanas P, Wigley DB (2000) DNA helicases: 'inching forward'. *Curr Opin Struct Biol* **10:** 124–128

Thoma NH, Czyzewski BK, Alexeev AA, Mazin AV, Kowalczykowski SC, Pavletich NP (2005) Structure of the SWI2/SNF2 chromatin-remodeling domain of eukaryotic Rad54. *Nat Struct Mol Biol* **12:** 350–356

Tirode F, Busso D, Coin F, Egly J-M (1999) Reconstitution of the transcription factor TFIIH: assignment of functions for the three enzymatic subunits, XPB, XPD, and cdk7. *Mol Cell* **3:** 87–95

Velankar SS, Soultanas P, Dillingham MS, Subramanya HS, Wigley DB (1999) Crystal structures of complexes of PcrA DNA helicase with a DNA substrate indicate an inchworm mechanism. *Cell* **97:** 75–84

Wang Z, Svejstrup JQ, Feaver WJ, Wu X, Kornberg RD, Friedberg EC (1994) Transcription factor b (TFIIH) is required during nucleotide-excision repair in yeast. *Nature* **368:** 74–76

White MF (2009) Structure, function and evolution of the XPD family of iron-sulfur-containing 5′→3′ DNA helicases. *Biochem Soc Trans* **37** (Part 3)**:** 547–551

Wolski SC, Kuper J, Hanzelmann P, Truglio JJ, Croteau DL, Van Houten B, Kisker C (2008) Crystal structure of the FeS cluster-containing nucleotide excision repair helicase XPD. *PLoS Biol* **6:** e149

Wu Y, Suhasini A, Brosh R (2009) Welcome the family of FANCJ-like helicases to the block of genome stability maintenance proteins. *Cell Mol Life Sci* **66:** 1209–1222

